Kinetic, spectroscopic and thermodynamic characterization of the *Mycobacterium tuberculosis* adrenodoxin reductase homologue FprA

Kirsty J. McLEAN, Nigel S. SCRUTTON and Andrew W. MUNRO[1]

Department of Biochemistry, University of Leicester, The Adrian Building, University Road, Leicester LE1 7RH, U.K.

The genome sequence of the pathogenic bacterium *Mycobacterium tuberculosis* revealed numerous cytochrome P450 enzymes, which require accessory redox enzymes for catalytic function (ferredoxin reductase and ferredoxin). The most likely ferredoxin reductase is encoded by *fprA*, and its structure resembles eukaryotic adrenodoxin reductases. We have cloned, expressed and purified the flavoenzyme product of the *fprA* gene in *Escherichia coli*. FprA reduces various electron acceptors using either NADPH or NADH as the electron donor, but discriminates in favour of NADPH (apparent K_m for NADH = 50.6 ± 3.1 μM; NADPH = 4.1 ± 0.3 μM from ferricyanide reduction experiments). Stopped-flow studies of reduction of the FprA FAD by NADPH demonstrate increased flavin reduction rate at low NADPH concentration (< 200 μM), consistent with the presence of a second, kinetically distinct and inhibitory, pyridine nucleotide-binding site, similar to that identified in human cytochrome P450 reductase [Gutierrez, Lian, Wolf, Scrutton and Roberts (2001) Biochemistry **40**, 1964–1975]. Flavin reduction by NADH is slower than with NADPH and displays hyperbolic dependence on NADH concentration [maximal reduction rate (k_{red}) = 25.4 ± 0.7 s^{-1}, apparent $K_d = 42.9 \pm 4.6$ μM]. Flavin reoxidation by molecular oxygen is more rapid for NADH-reduced enzyme. Reductive titrations show that the enzyme forms a species with spectral characteristics typical of a neutral (blue) FAD semiquinone only on reduction with NADPH, consistent with EPR studies. The second order dependence of semiquinone formation on the concentration of FprA indicates a disproportionation reaction involving oxidized and two-electron-reduced FprA. Titration of FprA with dithionite converts oxidized FAD into the hydroquinone form; the flavin semiquinone is not populated under these conditions. The midpoint reduction potential for the two electron couple is -235 ± 5 mV (versus the normal hydrogen electrode), similar to that for adrenodoxin reductase (-274 mV). Our data provide a thermodynamic and transient kinetic framework for catalysis by FprA, and complement recent spectrophotometric and steady-state studies of the enzyme [Fischer, Raimondi, Aliverti and Zanetti (2002) Eur. J. Biochem. **269**, 3005–3013].

Key words: adrenodoxin reductase, flavoprotein, FprA, potentiometry, stopped-flow kinetics.

INTRODUCTION

Mycobacterium tuberculosis (Mtb) currently represents one of the greatest threats to human health. The pathogenic bacterium causes the disease tuberculosis, and Mtb has undergone resurgence in recent years owing to proliferation of drug-resistant and multi-drug-resistant strains [1]. This has resulted in the global spread of a disease once thought almost eradicated. Mechanisms of resistance to the 'traditional' anti-tuberculosis drugs are becoming clear, and include down-regulation and mutational inactivation of Mtb drug-activating enzymes, e.g. the catalase/peroxidase encoded by *katG* required for isoniazid activation, and the *ethA* gene product for ethionamide [2,3]. Since a very limited range of antibiotics is effective against tuberculosis, the failure of these front line agents has very serious consequences for treatment of the disease. New drug therapies are desperately needed to counter the alarming spread of Mtb, and in this respect the recent determination of the genome sequence of Mtb has been a major breakthrough [4]. The genome sequence emphasizes the importance of lipid metabolism to Mtb, with a much larger number of lipid-metabolizing enzymes than is seen for other bacterial chromosomes of similar size.

The remarkable preponderance of cytochrome P450 mono-oxygenase (P450) enzymes (20 in Mtb compared with none in *Escherichia coli*) in the pathogen is probably due to cellular requirements for fatty acid and mycolipid oxygenating activities. The complexity of the Mtb lipid envelope is recognized as critical for the immunogenicity and drug resistance of the pathogen [5]. Structures of two of the Mtb P450s have been solved. These are the sterol demethylase homologue CYP51 (encoded by the *Rv0764c* gene) and CYP121 (encoded by *Rv2276*) [6,7]. CYP51 has been solved in a fluconazole-bound form. Fluconazole and other related azole drugs are used as both topical and systemic antifungal drugs, and are considered to exert their antibiotic action primarily by binding tightly and inactivating the fungal CYP51 enzyme. In recent studies, we have shown that azole antifungal drugs are potently effective as inhibitors of cell growth for *M. smegmatis* and the related actinomycete *Streptomyces coelicolor*, which also has an extensive complement of P450 enzymes [8,9]. We have also shown recently that the other structurally characterized Mtb P450 (CYP121) binds a series of azole antifungals more tightly than CYP51, and that the dissociation constants for the azole-P450 complexes correlate well with minimal inhibitory concentration values for the same drugs against *M. smegmatis*. CYP121 might therefore be a more likely target for azole drugs than CYP51 [9,10]. Should azole compounds have multiple cellular P450 targets in mycobacteria, the possible development of resistance would be much reduced.

P450s require one or more redox partners to deliver two electrons required for dioxygen cleavage and oxygenation of substrate [11]. In eukaryotic microsomal P450 systems (e.g.

Abbreviations used: AD, adrenodoxin; ADR, AD reductase; CT, charge transfer; DCPIP, 2,6-dichlorophenol-indophenol; DPI, diphenyliodonium; ESI-MS, electrospray ionization-MS; FprA, flavoprotein reductase A; H_4NADP, tetrahydro-NADP; Mtb, *Mycobacterium tuberculosis*; NOS, nitric oxide synthase; PDA, photodiode array; P450, cytochrome P450 mono-oxygenase; CPR, P450 reductase.

[1] To whom correspondence should be addressed (e-mail awm9@le.ac.uk).

the hepatic drug-metabolizing forms), electrons are delivered by the diflavin enzyme NADPH-P450 reductase (CPR) [12]. In bacteria and eukaryotic mitochondria, however, the redox system comprises a FAD-containing ferredoxin reductase and a ferredoxin [13]. In the mammalian mitochondrion, the NADPH-dependent adrenodoxin (AD) reductase (ADR) transfers electrons to AD, which, in turn, delivers electrons to P450 systems involved in steroid metabolism [14]. The atomic structures of ADR and AD have been solved, in isolation and in complex [15–17]. The protein encoded by *fprA* (*Rv3106*) in the Mtb genome is an ADR homologue and is likely to transfer electrons to some or all of the P450 systems. Given the proven potency of anti-P450 azole drugs against mycobacteria, targeting flavoprotein reductase A (FprA) to globally inactivate P450 redox function could provide an effective new antibiotic strategy. The atomic structure of FprA is known, and confirms a close structural relationship to rat ADR [18]. Fischer and co-workers [19] have reported the preliminary expression and characterization of FprA by steady-state kinetics and spectrophotometry. In the present study, we extend their work through a detailed spectroscopic, thermodynamic and stopped-flow kinetic study of FprA. Our studies reveal unusual properties of FprA, including an unusual inverse dependence of flavin reduction rate on [NADPH] that suggests the presence of a second (inhibitory) binding site for the cofactor. These and other novel features of the enzyme are discussed in respect to its catalytic properties and likely cellular role.

EXPERIMENTAL

Cloning and expression of *fprA*

The *fprA* gene (*Rv3106* from the Mtb genome project) encoding the FprA enzyme was amplified from the Mtb chromosomal DNA cosmid library (cosmid number MTCY339) obtained from Professor Stewart Cole at the Pasteur Institute, Paris. Primers were designed from the Mtb genomic sequence [4]: forward primer: 5′-TATGACTCATATGCGTCCCTATTACATCGCCATCG-3′; reverse primer: 5′-ATCCGGGATCCTCAGCCGAGCCCAATCCGCAACAGC-3′. In the forward primer, the underlined letters indicate an engineered site for restriction enzyme *Nde*I, incorporating the ATG initiation codon. In the reverse primer, the underlined letters indicate a *Bam*HI site, incorporating the TAG stop codon.

The PCR fragment containing the *fprA* gene was cloned into the plasmid vector pGEM-T (Promega), creating plasmid clone pKM3a. The DNA sequence of the cloned fragment was verified by automated DNA sequencing (Applied Biosystems DNA sequencer). The *fprA* gene was excised from pKM3a by digestion with *Nde*I and *Bam*HI, and ligated into the T7lac promoter vector pET11a (Novagen), which had been digested with the same enzymes. Plasmid constructs were selected by transformation of *E. coli* strain TG1 [20] and restriction digest of plasmids prepared from transformed cultures. The expression plasmid was designated pKM3b. All molecular biology procedures were performed using standard protocols [21].

Purification of FprA

The FprA enzyme was expressed in the T7 RNA polymerase lysogen strain HMS174 (DE3) (Novagen). HMS174 (DE3)/pKM3b transformants were grown at 30 °C with vigorous agitation (250 rev./min) until mid-logarithmic growth phase ($D_{600} \approx 0.8$–1.0) in Terrific broth [21]. The temperature was then decreased to 25 °C, and the culture induced by the addition of isopropyl β-D-thiogalactoside (1 mM). Culture growth was continued for a further 16–20 h. Cells (approx. 30–50 g wet weight) were harvested by centrifugation (7500 ***g***, 30 min, 4 °C), washed by resuspension in ice-cold 50 mM Tris/HCl (pH 7.2) containing 1 mM EDTA and 10 % (v/v) glycerol (buffer A), pooled and re-centrifuged. The final cell pellet was resuspended in a small volume of buffer A containing protease inhibitors PMSF and benzamidine hydrochloride (1 mM) and disrupted by sonication using a Bandelin Sonoplus GM2600 sonicator. The extract was passed three times through a French press (950 lbf/in^2, where 1 lbf/in^2 = 6.9 kPa) to complete cell breakage process and centrifuged at 18 000 ***g*** for 30 min (at 4 °C). Soluble extract was fractionated with ammonium sulphate (two steps: 0–30 % and 30–70 %); FprA was located in the 30–70 % pellet. The pellet was resuspended in buffer A/0.5 M ammonium sulphate and was applied on to a phenyl-Sepharose column (5 cm × 30 cm) pre-equilibrated in buffer A/1.5 M ammonium sulphate (buffer B). Protein was eluted using a linear gradient (500 ml) of buffer B to buffer A. FprA-containing fractions were loaded on to a Q-Sepharose column (5 cm × 25 cm) pre-equilibrated with buffer A. The column was developed using a linear gradient (500 ml) of buffer A to buffer A/500 mM KCl. FprA-containing fractions were then applied to a 2′,5′-ADP-Sepharose column (2 cm × 10 cm) pre-equilibrated with the same buffer. The column was washed extensively with buffer A, and FprA was eluted in buffer A/250 mM KCl. Fractions of highest purity ($A_{274}/A_{452} < 7.0$) were retained, pooled, concentrated by ultrafiltration (Centriprep 30; Millipore) to < 2 ml and exchanged into buffer A/50 % (v/v) glycerol by dialysis, prior to storage of the pure enzyme at − 80 °C.

The purity of FprA was assessed by spectral analysis (ratio of flavin-specific absorption at 452 nm compared with protein-specific absorption at 274 nm) and by SDS/PAGE of protein samples at different stages in the purification process. FprA concentration was determined from the flavin absorption maximum of the oxidized enzyme ($\varepsilon_{452} = 10.6$ mM$^{-1} \cdot$ cm^{-1} [19]).

The molecular mass of FprA was determined by electrospray ionization-MS (ESI-MS) using a micromass platform quadrupole mass spectrometer equipped with an electrospray ion source, as described previously [10]. The N-terminal sequence of FprA was determined by automated Edman degradation on an ABI 476 protein sequencer. FprA was exchanged into distilled water and concentrated to 5 mg $\cdot$ ml^{-1}, prior to sequencing at the Protein and Nucleic Acid Chemistry Laboratory facility at the University of Leicester.

UV-visible absorption spectroscopy and fluorimetry

UV-visible absorption spectra were recorded using a Cary UV-50 Bio UV-visible scanning spectrophotometer (Varian). Spectra were recorded for FprA [typically 5–10 μM in 10 mM sodium phosphate (pH 7.5); buffer C] in its oxidized form, and reduced in the presence of NADH, NADPH and sodium dithionite.

Flavin and tryptophan fluorescence spectra for FprA (5 μM) were recorded in buffer C using a Cary Eclipse fluorescence spectrophotometer (Varian). Flavin excitation was at 430 nm, and emission data were collected between 450 and 700 nm. Tryptophan excitation was at 290 nm, with emission data collected between 300 and 500 nm. Slit widths were set at 10 nm and 5 nm for excitation and emission respectively. Spectra were recorded for oxidized FprA, dithionite-reduced FprA and FprA in the presence of pyridine nucleotides and analogues thereof (5–50 μM of NAD$^+$, NADH, NADP$^+$, NADPH, NMN and 2′-AMP). The quantum yield (Q_f) for FAD fluorescence in FprA was determined

by measurement of FprA fluorescence under identical conditions with those used for analysis of fluorescence for free FAD, as described previously [22].

CD

CD spectra were recorded at 20 °C using a JASCO J600 spectrapolarimeter (calibrated with 0.06 % d-10 camphorsulphonic acid). Far-UV CD spectra were recorded over the wavelength range 190–260 nm in a quartz cylindrical cell of 0.02 cm pathlength (scan rate of 10 nm · min^{-1}). Near-UV and visible CD spectra were recorded over the wavelength ranges 260–320 nm and 320–600 nm respectively, in 0.5 cm pathlength cells (scan rates of 20 nm · min^{-1}). Spectra were recorded in duplicate and averaged. Protein concentrations used were 10.5 μM (far-UV), 58.5 μM (near-UV) and 175 μM (visible). All samples were in buffer C.

EPR spectroscopy

EPR spectra were recorded on an X-band ER-200B spectrometer (Bruker Spectrospin) interfaced to an ESP1600 computer and fitted with a liquid helium flow-cryostat (ESR-9; Oxford Instruments). Spectra were recorded at 50 K with 2 mW microwave power and a modulation amplitude of 1 mT. Protein samples (approx. 700 μM) were contained in 50 mM Hepes buffer (pH 7.5). Spectra were recorded for oxidized Fpr Aand for enzyme reduced with NADH, NADPH and sodium dithionite (10-fold molar excess).

Redox potentiometry

Redox titrations were performed in a Belle Technology glove-box under a nitrogen atmosphere, essentially as described previously [23]. All solutions were degassed under vacuum with argon. Oxygen levels were maintained at less than 2 parts per million. The protein solution [approx. 350 μM in 5 ml of 100 mM potassium phosphate buffer (pH 7.0), both in the absence and presence of 10 % (v/v) glycerol] was titrated electrochemically according to the method of Dutton [24] using sodium dithionite as reductant and potassium ferricyanide as oxidant. Mediators (2 μM phenazine methosulphate, 5 μM 2-hydroxy-1,4-naphthoquinone, 0.5 μM methyl viologen and 1 μM benzyl viologen) were included to mediate in the range between + 100 and − 480 mV, as described previously [23,25]. At least 15 min was allowed to elapse between each addition to allow stabilization of the electrode. Spectra (250–750 nm) were recorded using a Cary UV-50 Bio UV-Visible scanning spectrophotometer. The electrochemical potential of the solution was measured using a Hanna pH 211 meter coupled to a Pt/Calomel electrode (ThermoRussell Ltd) at 25 °C. The electrode was calibrated using the Fe^{3+}/Fe^{2+} EDTA couple as a standard (+ 108 mV). A factor of + 244 mV was used to correct relative to the standard hydrogen electrode. FprA redox titrations were repeated in the presence of tetrahydro-NADP (H_4NADP) at a concentration of 100 μM. The H_4NADP sample was a gift from Professor Rene Feyereisen and Dr Marat Murataliev (Department of Entomology, University of Arizona, Tucson, AZ, U.S.A.).

Steady-state kinetic analysis of FprA

The steady-state activity of FprA towards exogenous electron acceptors [2,6-dichlorophenol-indophenol (DCPIP) and ferricyanide] was determined spectrophotometrically using the Cary UV-50 Bio spectrophotometer. DCPIP reduction was measured at 600 nm ($\varepsilon_{600} = 21000\ M^{-1} \cdot cm^{-1}$), and (potassium) ferricyanide reduction at 420 nm ($\varepsilon_{420} = 1020\ M^{-1} \cdot cm^{-1}$). Reactions were performed in buffer C at 30 °C, typically using 0.05–1.0 μM FprA. Reaction progress was monitored over 1 min. Reaction rates were determined in triplicate at a variety of different concentrations of the electron acceptors and using NADPH and NADH as reductants. Data were fitted to a rectangular hyperbola using Origin software (Microcal) to derive K_m and k_{cat} values. Apparent K_m values for NADH and NADPH were determined by following reduction of ferricyanide and DCPIP (both at saturating concentrations, 2 mM and 100 μM respectively), over a range of NADH/NADPH concentrations.

Aerobic flavin reoxidation in FprA (30 μM) was monitored at 30 °C in buffer C following addition of a stoichiometric amount of NADPH. Reoxidation was measured through analysis of the rate of recovery of flavin absorption at 452 nm, fitting the absorption versus time data to an exponential function in Origin software.

Inhibition of FprA with the flavoenzyme suicide inhibitor diphenyliodonium chloride (DPI; Aldrich) was measured in steady-state reactions by following NADPH-dependent reduction of ferricyanide and of DPI itself. In ferricyanide reductase assays, the rate of absorption decrease at 420 nm was followed in a system containing 0.039 μM FprA, 1 mM ferricyanide and DPI between 0.2–10 mM. Reactions were performed at 30 °C in buffer C and initiated by addition of 200 μM NADPH. For reactions using DPI as the substrate, reactions were performed in the same way, but with a higher enzyme concentration (0.78 μM FprA) and by measuring the rate of NADPH oxidation at 340 nm ($\varepsilon_{340} = 6.21\ mM^{-1} \cdot cm^{-1}$).

Rates of enzyme inactivation were determined by fitting individual progress curves to equation 1:

$$v = \frac{V_o(1 - e^{-k_{obs}t})}{k_{obs}} + at \quad (1)$$

as described previously [26], where v is the observed rate at time t, V_o is the initial reaction rate, k_{obs} is the rate of enzyme inactivation and a is a linear term to correct for residual enzyme activity through incomplete inhibition.

Stopped-flow kinetic studies of FprA

Stopped-flow studies of FprA reduction were performed under anaerobic conditions using an Applied Photophysics SX18MV stopped-flow instrument, at 30 °C in buffer C. FprA (5 μM) was mixed in the stopped-flow apparatus with either NADH or NADPH (in the range 0–2 mM), and bleaching of the flavin monitored at its absorption maximum (452 nm). Reaction transients were described by a single exponential process and observed rates were calculated using Spectrakinetics software (Applied Photophysics). Analysis of the concentration dependence of the reaction rate is described in the Results section.

The UV-visible absorption spectra of FprA formed during reduction of the enzyme (40 μM) with NADH and NADPH (40 μM and 400 μM) were collected using a photodiode array (PDA) attachment in rapid mixing experiments. Spectra were accumulated over various time periods following the mixing event. Spectra were analysed globally, using the Applied Photophysics ProKin software package, to identify distinct intermediate spectral forms and to define their rates of formation.

The ability of dithionite-reduced FprA to pass electrons to $NADP^+$ was also investigated. FprA (approx. 1 mM) was made

anaerobic and reduced by addition of excess sodium dithionite in the glove box. The enzyme was separated from reductant by gel filtration using a BioRad Econo-Pac 10DG desalting column in the anaerobic box, pre-equilibrated with degassed buffer C. The reduced enzyme was diluted to 20 μM and mixed with NAD^+ or $NADP^+$ (50 μM, 200 μM and 1 mM) in the stopped-flow apparatus. Measurements of the rate of reverse electron transfer were made both in single wavelength mode (452 nm) and using a PDA detector. Reoxidation of FprA (approx. 30 μM, pre-reduced with stoichiometric dithionite and gel filtered in the glove box) in the presence of NAD^+ and $NADP^+$ (various concentrations up to 1 mM) was analysed by the stopped-flow method using single wavelength and PDA detection. Data analysis was as described above for the reductive half-reaction.

For NADPH-dependent reduction of FprA, the influence of protein concentration on the rate of development of the FAD semiquinone was determined at 575 nm by mixing NADPH (1 mM) and FprA (6, 10, 20, 30, 50, 100 and 150 μM) in the stopped-flow instrument. Data were fitted to a single exponential function. Observed rates were plotted versus FprA concentration.

Stopped-flow fluorescence experiments employed an excitation wavelength of 340 nm (NADPH); the emission band at 450 nm was selected using a bandpass filter (Coherent Optics); NADH and NADPH concentration was 5–50 μM; FprA concentration was 5 μM. Reactions were carried out at 25 °C in buffer A under anaerobic conditions.

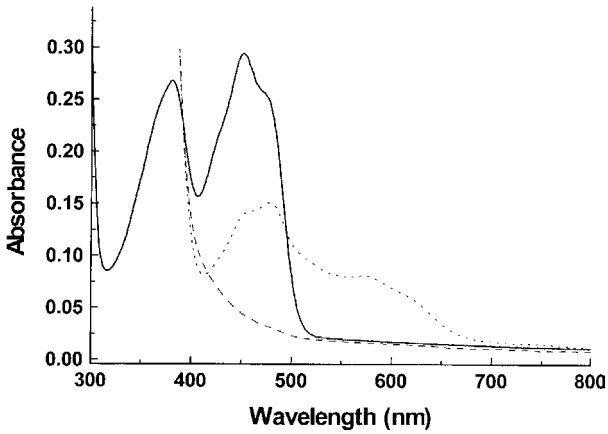

Figure 1 UV-visible spectral properties of FprA

FprA exhibits spectral features typical of flavin-binding enzymes, but unusual properties as regards the extent of reduction induced by addition of various reductants. The Figure shows the visible absorption spectra for pure FprA (26 μM) in its oxidized (solid line), NADPH-reduced (dotted line) and NADH-reduced (broken line) forms. For both NADPH and NADH, a 10-fold molar excess of reductant was added. The NADPH-reduced enzyme has distinct maxima at approx. 478 nm and 575 nm, with a large shoulder at 453 nm. All visible flavin absorption is bleached for the NADH-reduced form. The sodium dithionite-reduced FprA (results not shown) had visible absorption features identical with that for the NADH-reduced enzyme (i.e. completely hydroquinone flavin).

Materials

Oligonucleotide primers for PCR were obtained from PerkinElmer Applied Biosystems, or were manufactured at the Protein and Nucleic Acid Chemistry Laboratory at the University of Leicester. All restriction enzymes and DNA modifying enzymes were from New England Biolabs. Other modifying enzymes, *Taq* and *Pfu* DNA polymerase and T4 DNA ligase were obtained from Promega. Spinach ferredoxin was purchased from Sigma (Poole, Dorset, U.K.). *E. coli* flavodoxin was prepared as described previously [27]. Unless otherwise stated, all reagents used (including NADH and NADPH) were obtained from Sigma and were of the highest grade available. Media and solutions were made according to standard procedures [21].

RESULTS

General properties of FprA

The *fprA* gene was initially expressed at high levels in a variety of *E. coli* T7 RNA polymerase lysogen strains but, as observed previously for cytochrome P450 enzymes from Mtb [7,10], a large proportion of the protein product was found to form inclusion bodies. Soluble FprA was obtained by expression of the gene in the *E. coli* strain HMS174 (DE3) [28,29], as described in Experimental section. The expression of FprA was not compromised at lower growth temperature (25 °C), but this greatly increased the production of soluble FprA compared with growth at 37 °C.

FprA was purified approx. 10-fold from the original cell extract, and the ratio of total protein to flavin-specific absorption (i.e. A_{274}/A_{452}) was 6.8. Purified samples were judged to be homogeneous by SDS/PAGE. The molecular mass (49 357 $\pm$ 25 Da; expected mass 49 346 Da) of FprA estimated by EMI-MS indicates the lack of post-translational modification of the enzyme and retention of the N-terminal methionine residue. Automated Edman degradation indicated that the N-terminal sequence of pure FprA protein (Met-Arg-Pro-Tyr-Tyr-Ile) was identical with that predicted from the gene sequence (Tuberculist World-Wide Web Server at: http://genolist.pasteur.fr/TubercuList/).

The pure FprA enzyme in its oxidized state exhibits spectral features typical of flavin-containing enzymes, with spectral maxima at 274 nm, 380 nm and 452 nm (Figure 1). Shoulders on the longer wavelength band are located at 425 nm and 473 nm. The protein/flavin absorption ratio ($A_{274}/A_{452} = 6.8$) compares favourably with values reported previously for ADRs purified from bovine adrenal gland ($A_{272}/A_{450} = 8.40$) [30] and from rat liver ($A_{269}/A_{450} = 7.25$) [31]. Addition of excess sodium dithionite or NADH under anaerobic conditions induces full reduction of the FAD, with complete bleaching of the flavin spectrum and without formation of spectral signals attributable to flavin semiquinone species. However, addition of excess NADPH (up to 1 mM) does not bring about complete flavin reduction, as observed also by Fischer et al. [19]. Instead, there is partial bleaching of the oxidized flavin spectrum and the development of an absorption band centred at 575 nm, as observed typically for neutral, blue flavin semiquinones {e.g. [27,32] and (Figure 1)}.

The far-UV CD spectrum of FprA (Figure 2, spectrum A) is typical of enzymes with considerable content of both α-helix and β-sheet [18]. The atomic structure of FprA indicates that the enzyme has approx. 42 % α-helix and 26 % β-sheet. NADPH, NADH and dithionite reductants and $NADP^+$ did not alter the far-UV CD spectrum of FprA, indicating negligible effect on secondary structure. In the near-UV region (260–320 nm; Figure 2, spectrum B), the spectrum is finely structured, with negative ellipticity between 260–281 nm, and a positive CD signal between 281–314.5 nm. In the visible CD spectrum (320–600 nm; Figure 2, spectrum C), there is also fine structure relating mainly to the chiral signal from the FAD cofactor. CD minima are located at 451 nm (close to the electronic absorption maximum at 452 nm) and at 469 nm. The visible CD spectrum is similar in overall shape to that reported previously for the *E. coli* flavodoxin (ferredoxin) reductase ('FLDR') [32]. The visible CD spectrum for FprA provides a unique 'fingerprint' for the enzyme, with characteristics more clearly distinguishable from

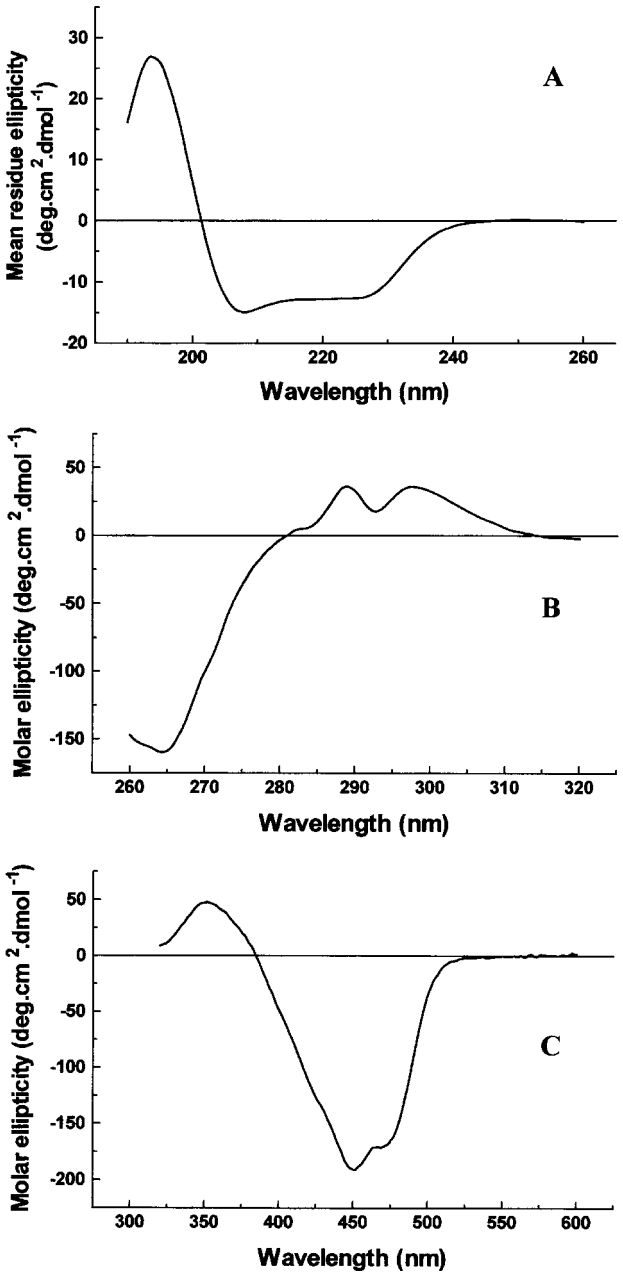

Figure 2 CD spectra for Mtb FprA

CD spectra for oxidized FprA are shown. (**A**) Far-UV CD spectrum (190–260 nm) recorded using 10.5 μM FprA (0.517 mg · ml^{-1}). Molar ellipticity is in units of deg · cm^2 · dmol^{-1}. (**B**) Near-UV CD spectrum (260–320 nm) recorded using 58.3 μM FprA (2.87 mg · ml^{-1}). (**C**) Visible CD spectrum (320–600 nm) recorded using 174.9 μM FprA (8.62 mg · ml^{-1}). Spectra were collected as described in the Experimental section.

other flavoproteins than those provided by UV-visible absorption spectra.

EPR spectra were recorded for FprA (approx. 700 μM) reduced anaerobically in the presence of excess dithionite, NADH and NADPH (10-fold excess in all cases). The results confirm that the spectral species observed in UV-visible absorption studies for NADPH-reduced enzyme (with absorption maximum at 575 nm) is the neutral, blue semiquinone form of the FAD. Integration of the EPR signal indicated that the radical resulted from approx. 30 % of the total FprA protein sample. However, negligible flavin semiquinone was detected for FprA reduced by either NADH

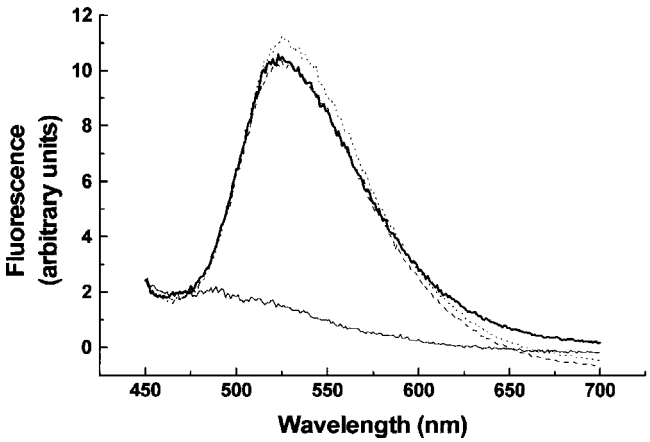

Figure 3 Flavin fluorescence from oxidized and reduced forms of FprA

Fluorescence spectra were recorded on a Cary Eclipse fluorescence spectrophotometer (Varian) using cells of pathlength 1 cm, with slit widths set at 10 nm (excitation) and 5 nm (emission) on the instrument. Protein samples were at a final concentration of 5 μM in buffer C and spectra were recorded for the oxidized FprA (thick solid line) and for the enzyme reduced using dithionite (thin solid line), NADH (broken line) and NADPH (dotted line; all at 50 μM), as described in the Experimental section.

or sodium dithionite, which both reduce FprA fully to its EPR-silent hydroquinone form. An excess of the powerful reductant dithionite would be expected to reduce the flavin completely. However, it should be noted that a progressive redox titration of FprA with dithionite (see below) also failed to produce any semiquinone spectral signal. It is unusual, therefore, that NADPH, which is an obligate two-electron donor, is capable of producing flavin semiquinone under anaerobic conditions, whereas NADH [with identical midpoint reduction potential (E°) to NADPH, E° = – 320 mV] does not produce flavin semiquinone.

Analysis of FprA FAD fluorescence (Figure 3) showed that it was extensively quenched in the protein matrix, as usually found for flavoenzymes [22]. Using fluorescence excitation at 430 nm (near the flavin absorption maximum), the emission maximum was located at 525 nm. By comparison with the fluorescence measured for free FAD under identical conditions, the quantum yield for the flavin fluorescence emission from FprA was 0.01 (0.03 for the free FAD [22]). Dynamic deactivation of excited FAD by the adenosine moiety is well known for FAD in aqueous solution. However, despite the relatively extended structure of the flavin cofactor in the FprA protein [18], the quantum yield of enzyme-bound FAD is one-third of that seen for FAD in solution. As expected for a hydroquinone, flavin fluorescence was essentially lost on the addition of dithionite. However, flavin fluorescence signals of similar intensity and wavelength maximum to those for the oxidized enzyme were obtained with FprA in the presence of either NADH (50 μM) or NADPH (5–50 μM) (Figure 3). Full reduction of FprA was achieved on adding 50 μM NADH (Figure 1), but the flavin emission spectrum was almost identical with the emission spectrum of oxidized FprA. The reduction state of the flavin was checked after fluorescence measurements to ensure maintenance of the reduced state. In the presence of NADP$^+$, 2′-AMP and NMN, the flavin fluorescence was essentially identical with ligand-free oxidized FprA.

Reduction potential of FprA

The reduction potentials of the FAD couples in FprA were determined by anaerobic spectroelectrochemical titration, as described previously [23,33]. In preliminary redox titrations of

FprA, it was found that the enzyme aggregated and precipitated over the several hours required to complete the titration [34]. This prevented accurate determination of the reduction potential of FprA, but did indicate clearly that there was negligible formation of the neutral, blue semiquinone form of the FAD flavin during either the reductive reaction with dithionite or on flavin reoxidation using ferricyanide. Thus, the semiquinone is destabilized with respect to the hydroquinone form under equilibrium titration conditions. Since the quality of the data collected from redox titrations of ligand-free FprA deteriorated with time owing to enzyme aggregation, titrations were performed over a much shorter time interval, during which 15 data points were collected over 1 h across the entire range from oxidized-to-reduced FprA. In this case, a fit of apparent absorption change (having baseline corrected for absorption increases due to turbidity in the final few samples) at the flavin maximum (A_{453}) against applied potential to a 2-electron Nernst function gave a midpoint potential of -230 ± 12 mV for the oxidized/hydroquinone transition. The redox titration was repeated in buffer containing 10% (v/v) glycerol, which slowed the aggregation process. In this case, the redox properties of the enzyme were found to be essentially identical with those in the absence of glycerol.

In further redox titration experiments, we examined the behaviour of the enzyme in the presence of the NADPH analogue H_4NADP, a redox-inactive hydrogenated derivative of NADPH [35]. Through use of H_4NADP, we sought to investigate redox behaviour of the FprA FAD for the pyridine nucleotide-bound form of the enzyme. Surprisingly, we found that, in the presence of 500 μM H_4NADP (K_d for NADPH is $< 5\,\mu$M), the enzyme did not aggregate to any significant extent during a full redox titration (Figure 4A). This facilitated a complete investigation of the redox properties of the FAD, and demonstrated again more clearly that there was no significant formation of a neutral, blue semiquinone during reductive/oxidative titrations with dithionite/ferricyanide. By fitting absorbance data collected at 453 nm to the 2-electron Nernst function, a clear transition between oxidized and hydroquinone forms is apparent, without inflexion of the curve that would indicate population of a semiquinone species. Thus the individual reduction potentials for the oxidized/semiquinone and semiquinone/hydroquinone couples are not distinguishable (although the potential for the semiquinone/hydroquinone transition may be more positive than that for oxidized/semiquinone). The midpoint reduction potential for H_4NADP-bound FprA was determined as -235 ± 5 mV, similar to that predicted for the ligand-free form (Figure 4B).

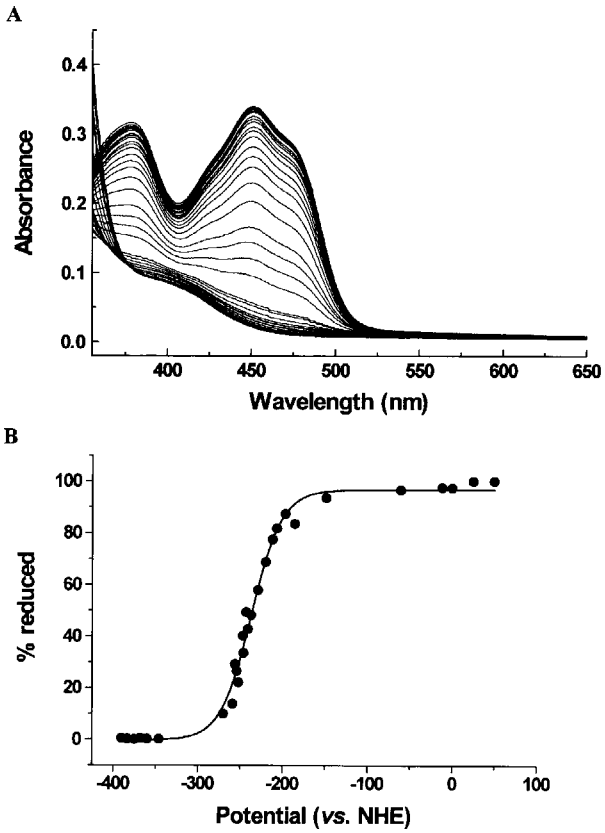

Figure 4 Potentiometric analysis of FprA

Anaerobic spectroelectrochemical titrations were performed as described in the Experimental section. (**A**) Representative spectra for the conversion of H_4NADP-bound FprA (approx. 30 μM) between oxidized and hydroquinone forms using dithionite reductant and ferricyanide oxidant. No spectral signals typical of the blue semiquinone form of the FAD flavin accumulate during reductive or oxidative titrations. (**B**) Plot of the percentage of the enzyme reduced (from ΔA_{453} data) versus the reduction potential (corrected versus normal hydrogen electrode) for the redox titration performed in the presence of H_4NADP. The data are fitted to a 2-electron Nernst function, yielding a midpoint reduction potential of -235 ± 5 mV for the oxidized/hydroquinone transition.

Kinetic properties of FprA

Reductase activities for FprA towards the electron acceptors DCPIP and ferricyanide were determined in steady-state assays. In preliminary experiments using ferricyanide, the preference of FprA for NADPH over NADH was established, and assays to determine the K_m and k_{cat} values for the electron acceptors were performed at saturating concentrations of NADPH (200 μM). Reactions with ferricyanide and DCPIP obeyed Michaelis–Menten behaviour and fits of the data to rectangular hyperbolae yielded the relevant kinetic parameters. The reduction of ferricyanide ($k_{cat} = 33.7 \pm 1.7\ s^{-1}$, $K_m = 160.3 \pm 26.8\,\mu$M) is much faster than that of DCPIP ($k_{cat} = 2.5 \pm 0.1\ s^{-1}$, $K_m = 10.7 \pm 1.1\,\mu$M). However, the overall catalytic efficiency of the two reactions is similar owing to a smaller K_m value for DCPIP ($k_{cat}/K_m = 0.21 \pm 0.06\,\mu M^{-1} \cdot s^{-1}$ for ferricyanide compared with $0.23 \pm 0.03\,\mu M^{-1} \cdot s^{-1}$ for DCPIP). Catalytic parameters were not altered significantly when reduction rates of ferricyanide and DCPIP acceptors were re-measured at 50 μM NADPH. Apparent K_m values for NADH and NADPH were obtained by re-determining ferricyanide reduction rates at a fixed saturating concentration of the electron acceptor (1 mM) and by varying the concentration of NADH (0–1 mM) and NADPH (0–200 μM) electron donors in the assays. The K_m values obtained for NADPH/NADH were $4.1 \pm 0.3\,\mu$M/$50.6 \pm 3.1\,\mu$M respectively.

In view of the potential of FprA as a drug target [36], we investigated inhibition of the enzyme using the flavoenzyme suicidal inhibitor DPI. For reactions performed with DPI as the sole electron acceptor, the apparent K_m value for DPI was determined as 8.9 ± 0.7 mM. The maximal rate of enzyme inactivation was determined as $0.023 \pm 0.002\ s^{-1}$ by fitting individual progress curves to eqn (1), as described previously [26]. The maximal rate of FprA inactivation ($0.023\ s^{-1}$) is lower than that reported previously for rat CPR ($0.087\ s^{-1}$) [26]. In a parallel set of reactions, the effect of DPI on the ferricyanide reductase activity of FprA was measured. However, DPI did not inhibit activity of FprA in this case, probably reflecting higher affinity and accessibility of ferricyanide (compared with DPI) to the FAD.

Transient kinetics and PDA studies

Stopped-flow absorption spectroscopy under anaerobic conditions was used to examine the reductive half reactions of FprA, using both NADH and NADPH as reductants. The hydride transfer reaction was followed at 452 nm (the flavin absorption maximum) following stopped-flow mixing of FprA and the reduced pyridine nucleotide cofactors. The reactions were seen to be markedly different. In the case of NADH, a hyperbolic dependence of reduction rate on [NADH] was described, with hydride transfer rate increasing at higher [NADH]. A fit of the data points to a rectangular hyperbola generates an apparent K_d value of $42.9 \pm 4.6\ \mu$M and a maximal reduction rate (k_{red}) of $25.4 \pm 0.7\ s^{-1}$. The reductive reaction with NADPH occurred at a similar rate to the k_{red} for NADH ($20 \pm 2\ s^{-1}$) for NADPH concentrations between 200 μM and 2 mM. However at [NADPH] $\leqslant 200\ \mu$M, there was a dramatic and progressive increase in reduction rate, such that the rate at 25 μM NADPH was $43.6\ s^{-1}$, and at 6.25 μM NADPH it had risen to $122.8\ s^{-1}$ (Figure 5). The apparent inverse dependence of reaction rate versus [NADPH] is similar (although more pronounced) to that observed recently for the diflavin enzymes CPR and nitric oxide synthase (NOS) [37,38].

In view of the unusual reduction behaviour observed with NADPH compared with NADH, we also examined the reverse electron transfer reaction between dithionite-reduced FprA and $NAD^+/NADP^+$. In the case of NAD^+, there was negligible reverse electron transfer to form NADH. However, with $NADP^+$ there was rapid flavin reoxidation. In reactions where 20 μM FprA was mixed with either 50 μM, 200 μM or 1 mM $NADP^+$, rates for flavin reoxidation (measured at 575 nm) were consistently similar at $340 \pm 30\ s^{-1}$. Thus, despite the thermodynamic barrier (midpoint reduction potential for $NADP^+$/H couple $= -320$ mV versus -235 mV for the $FAD/FADH_2$ couple), the flavin reoxidation reaction occurs rapidly.

Under aerobic conditions in the presence of a stoichiometric quantity of NADPH, there were marked differences in the rate of reoxidation of FprA (30 μM). For NADH, reoxidation was complete within 3 min, with a reoxidation rate of $4.83 \times 10^{-3} \pm 3.33 \times 10^{-4}\ s^{-1}$. However, reoxidation of the NADPH-bound form was markedly slower, with full recovery of the oxidized FprA spectrum taking > 3 h, with a rate of $< 8 \times 10^{-5}\ s^{-1}$.

The entire spectral changes occurring during reduction of FprA (40 μM) with either NADH or NADPH (stoichiometric or 10-fold excess) were recorded by stopped-flow using the PDA attachment on the Applied Photophysics instrument, over a variety of time scales following the mixing event. The data for NADPH confirm the findings from the single-wavelength study, i.e. that the reductive reaction proceeds more rapidly at lower concentrations of NADPH. The final spectra accumulated with 10-fold excess NADPH over short time regimes (i.e. < 300 ms) resemble that shown in Figure 1 (Figure 6A), i.e. with long wavelength spectral features typical of flavin semiquinone. In this time regime, the data for stoichiometric NADPH fit to a single step model ($A \rightarrow B$), but those for $10 \times$ NADPH require a third species ($A \rightarrow B \rightarrow C$) for a good fit to the data, with approx. 80 % of the amplitude in the initial (fast) phase and the slow phase consistently occurring at $< 0.5\ s^{-1}$. When absorption spectra were collected over much longer time regimes (100–1000 s), a multi-step model was required, due to subsequent slow reactions, perhaps involving electronic comproportionation between different FprA species. Using stoichiometric NADH, reduction was slower than with NADPH and did not progress to full reduction of the FAD. However, the nature of the flavin spectrum indicated that only oxidized and hydroquinone species were present. At 10-fold excess of NADH, the near complete

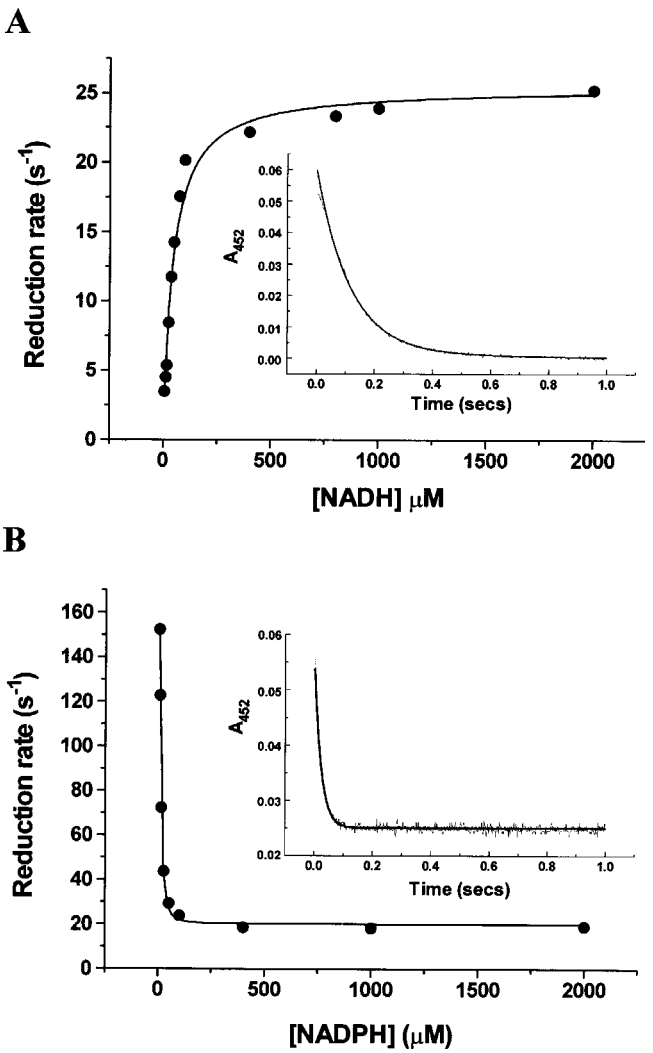

Figure 5 Stopped-flow single-wavelength absorption analysis of NADH- and NADPH-dependent flavin reduction in FprA

The rate of hydride transfer to the FprA FAD flavin was monitored by absorption change (decrease) at the oxidized flavin maximum (452 nm). Stopped-flow mixing of NADH and NADPH (0–2 mM) with FprA (5 μM) was performed anaerobically, as described in the Experimental section. The reduction rates derived from single exponential fits of the absorption versus time data against the relevant [NADH] (**A**) and [NADPH] (**B**) are plotted. For the NADH data, the points are fitted to a rectangular hyperbola. For the NADPH data, points are fitted to an exponential decay function in Origin software. Insets, individual representative traces (single exponential fits to data shown as solid black lines) at 25 μM NADPH. The respective reduction rates determined are $43.6\ s^{-1}$ (NADPH) and $8.4\ s^{-1}$ (NADH).

conversion to FAD hydroquinone was observed within 300 ms of the mixing event. Over this time frame, the NADH reduction data fitted best to a three-step model ($A \rightarrow B \rightarrow C$), with approx. 95 % of the amplitude in the rapid first phase and the slow phase again occurring consistently at $< 0.5\ s^{-1}$ (Figure 6B). The rates measured in PDA mode for the fast phases in both NADH- and NADPH-dependent FprA reductions are similar to those obtained in single-wavelength stopped-flow (see above).

PDA detection was used also to follow spectral changes occurring following mixing of dithionite-reduced (hydroquinone) FprA with $NADP^+$ and NAD^+ (see above). PDA data collected in these experiments were consistent with the single-wavelength studies at 452 nm, showing rapid flavin reoxidation in the FprA sample (rate $> 300\ s^{-1}$) on mixing with $NADP^+$ (Figure 6C), and negligible spectral change on mixing with NAD^+ (Figure 6D). The

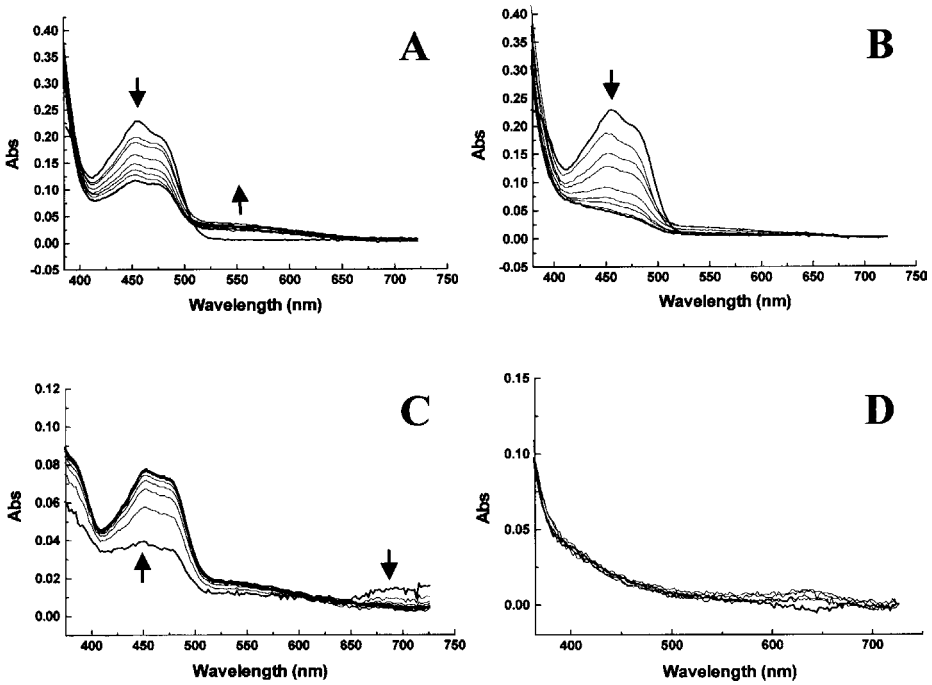

Figure 6 PDA UV-visible absorption spectra for reductive and oxidative reactions of FprA

UV-visible absorption (Abs) spectra accumulating during the anaerobic reduction and reoxidation of FprA were collected as described in the Experimental section. Data were analysed using the Photophysics ProKin software package to identify distinct spectral intermediates in the reactions. Spectra are shown for the reductive half reaction of FprA (22 μM) with 10-fold excess of NADPH (**A**) and NADH (**B**). The upper thick line is the first spectra collected (0.00128 s) and the lower thick line the spectrum collected 0.2547 s after mixing (after which negligible further change was observed). Intermediate spectra are shown as thin lines. Arrows indicate direction of absorption change at the flavin maximum and at approx. 575 nm (neutral, blue semiquinone). (**C** and **D**) Reoxidation of dithionite-reduced FprA (12 μM) with 30 μM $NADP^+$ and 500 μM NAD^+ respectively. In (**C**), the lower thick line is the first spectra collected at 0.0064 s and the upper thick line lower solid line the spectrum collected 0.0384 s after mixing (after which negligible further change was observed). Intermediate spectra are shown as thin lines. Arrows indicate direction of absorption change at the flavin maximum and at approx. 700 nm (putative charge transfer band). In (**D**), the thick line is the first spectrum collected (0.0064 s) with thin lines showing subsequent spectra up to 1000 s after mixing.

final spectra collected for oxidized FprA reduced with NADPH, or hydroquinone FprA reoxidized with the same [$NADP^+$], were virtually identical, indicating that the same end point is reached in either oxidative (hydroquinone FprA plus $NADP^+$) or reductive (oxidized FprA plus NADPH) directions.

In view of (in the case of NADPH) the complex nature of the absorption changes that occur on a rapid timescale following mixing of pyridine nucleotide cofactor with FprA, we analysed also the fluorescence change associated with oxidation of NADPH following stopped-flow mixing with FprA. Figure 7 shows the nicotinamide fluorescence changes (excitation at 340 nm, emission at 450 nm) observed following mixing of FprA with stoichiometric (5 μM) and 10-fold excess (50 μM) NADPH. The transients observed on mixing with stoichiometric NADPH are biphasic, with the first rate similar to that observed by stopped-flow flavin absorption measurements (6.1 s^{-1} and 1.1 s^{-1} for NADH; 30.0 s^{-1} and 1.8 s^{-1} for NADPH) (Figures 7A and 7C respectively). In both cases, approx. 60 % of the overall amplitude change occurred in the first phase. For NADH at 50 μM, the data fit best to a single exponential function (25.2 s^{-1}; Figure 7B). However, for NADPH at 50 μM (Figure 7D), following an initial fast decrease in nicotinamide fluoresecence (as seen in the other traces), there is an increase in fluorescence, followed by a slower decrease. The slower fluorescence changes over the longer timebase probably reflect comproportionation between different NADPH/$NADP^+$-bound forms of FprA, as described in the Discussion.

EPR studies of NADPH-reduced FprA indicated only the presence of a flavin radical (see above). In the absence of a protein radical signal, the semiquinone species formed under anaerobic conditions should reflect comproportionation between oxidized and reduced (hydroquinone) molecules of FprA. To investigate this, we measured rates of semiquinone formation (ΔA_{575}) in the stopped-flow instrument, following mixing of oxidized FprA (6–150 μM) with NADPH (fixed at 1 mM). Semiquinone formation rate showed a linear dependence on [FprA], with a second order rate constant of $9.82 \times 10^{-3} \pm 1.0 \times 10^{-4}$ $s^{-1} \cdot \mu M^{-1} \cdot$ FprA (Figure 8).

DISCUSSION

FprA is the first homologue of eukaryotic ADR characterized in a prokaryote. The recent determination of its atomic structure reveals extensive similarity with the previously determined structure of rat ADR [18]. ADR is located in the mitochondrial membrane and passes electrons from NADPH to the Fe_2S_2 iron–sulphur protein AD [16]. In turn, AD shuttles electrons one-at-a-time to mitochondrial P450 systems involved in steroid synthesis and inter-conversions, perhaps most notably the cholesterol side-chain cleavage enzyme P450scc (or CYP11A1 in the systematic nomenclature system derived by Nelson) [39,40]. A similar situation is likely to occur in the Mtb cytoplasm (or at the cytoplasm/inner membrane boundary), with FprA providing NADPH-derived electrons to several cytochrome P450 systems involved in lipid metabolism [10]. There are potentially a number of ferredoxin-like proteins encoded in the Mtb genome that might act as electron carriers between FprA and the P450s. One of these (the product of gene *Rv0763c*) has been characterized as a Fe_3S_4

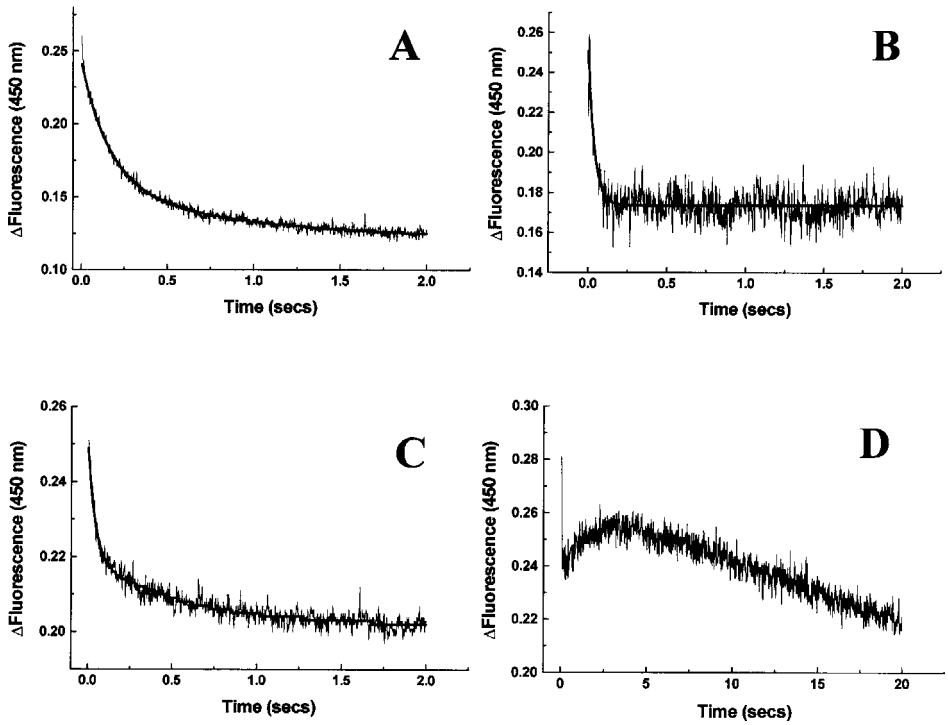

Figure 7 Stopped-flow nicotinamide nucleotide cofactor fluorescence changes on mixing of NADPH with FprA

The fluorescence changes associated with oxidation of NADPH were monitored on stopped-flow mixing of FprA (5 μM) with stoichiometric NADH (**A**) and NADPH (**C**), and 10-fold excess (50 μM) NADH (**B**) and NADPH (**D**). In (**A**) and (**C**), data are fitted to a double exponential function, with the fit line shown as a solid black line through the data. In (**B**), the fit line represents a single exponential fit through the data.

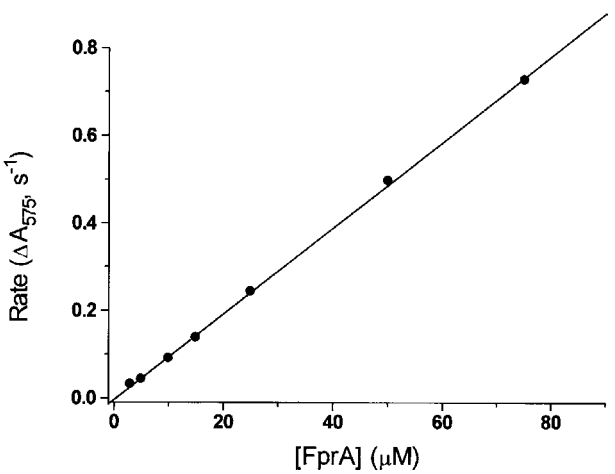

Figure 8 Protein concentration dependence of flavosemiquinone formation rate on NADPH-dependent reduction of FprA

Rates of semiquinone formation were measured at 575 nm following stopped-flow mixing of FprA (6–150 μM) with NADPH (1 mM). Rates are plotted versus the relevant [FprA] and a linear fit of the data yields a second-order rate constant of 0.589 ± 0.006 $min^{-1} \cdot \mu M^{-1}$ · FprA.

ferredoxin and shown to mediate electron transfer to one of the Mtb P450s (CYP51) [41].

In the current study, we present a detailed kinetic and thermodynamic characterization of FprA, an enzyme that displays some unusual characteristics. Most notable is the capacity of NADPH to reduce the enzyme only partially and to produce a blue semiquinone intermediate. This contrasts with NADH, which reduced the FAD cofactor completely to its hydroquinone form. In addition, the rate at which NADH and NADPH transfer hydride ions to the FAD differs, as does the dependence of this rate on the concentration of the pyridine nucleotide cofactors. Although the rate dependence on [NADH] is positive and hyperbolic, there is negligible dependence on [NADPH] between 200 μM and 2 mM, where hydride transfer takes place at a rate similar to the maximal rate determined for NADH-dependent reduction (i.e. approx. 20 s^{-1}). However, at low [NADPH], there is a marked increase in hydride transfer rate, with the rate increasing dramatically as the [NADPH] is decreased below 200 μM (Figure 5B). This type of inverse rate dependence on [NADPH] has been recognized previously in mammalian CPR and (to a lesser extent) in NOS [12,38,42]. However, the effect is much more pronounced with FprA. In the case of human CPR, the acceleration of hydride transfer observed at low [NADPH] was rationalized in terms of two binding sites for pyridine nucleotide, one catalytic and one regulatory. Population of the regulatory binding site interferes with hydride transfer in the catalytic site and possibly obstructs the dissociation of $NADP^+$ product [12]. A similar situation may also operate for FprA. The fact that NADH and NADPH induce very different degrees of flavin reduction in FprA (despite their having identical reduction potential -320 mV) points strongly to the importance of the additional 2′-phosphate group in NADPH in controlling binding and flavin reduction. Clearly, with FprA, further detailed spectroscopic and kinetic studies coupled with analysis of site-directed mutants are needed in order to probe further the unusual regulatory effects imposed by NADPH. However, with only a single flavin involved, the mechanistic aspects may prove easier to deconvolute than in CPR, where electron transfer reactions are complicated by the inter-flavin electron exchange. The proposed intermediates

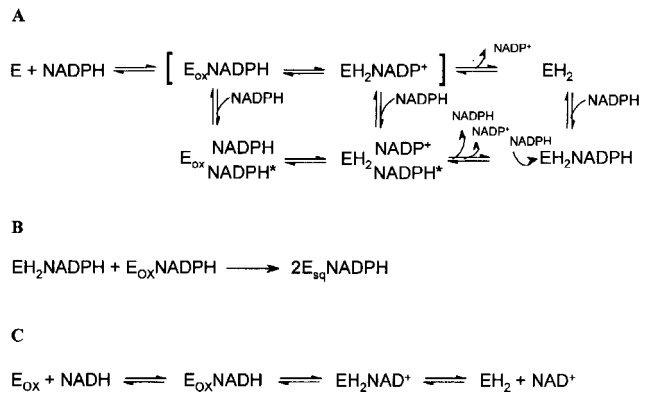

Scheme 1 Proposed intermediates in the reactions of FprA with NADH and NADPH cofactors

in the NADPH- and NADH-dependent reduction of FprA are detailed in Scheme 1.

In our proposed scheme for the interaction of NADPH with FprA (Scheme 1A), the first event is the binding of NADPH to the oxidized enzyme (E_{ox}), forming a transient charge transfer (CT) intermediate. The CT species encompasses E_{ox}NADPH and EH_2NADP^+ in our scheme (i.e. the species enclosed by square brackets). The CT species collapses after hydride transfer when $NADP^+$ dissociates. Dissociation of $NADP^+$ leaves the hydroquinone (EH_2) form of FprA. This section of the scheme is similar to that proposed for the reaction with NADH (Scheme 1C) and to that suggested by Fischer et al. [19]. However, the NADPH-dependent reaction is complicated by the capacity of NADP(H)-bound FprA to interact with a second molecule of NADPH (indicated by NADPH*), which occupies the regulatory site that modulates the reactivity of FprA. The second molecule of NADPH can bind to either NADPH-bound E_{ox} or $NADP^+$-bound EH_2 forms of FprA, which we consider to be in a dynamic equilibrium (i.e. the CT species, as also proposed by Fischer et al. [19]). As recognized through studies of CPR and NOS, $NADP^+$-release is an important rate-limiting step in the catalytic reaction of these enzymes [12,42], and we consider that the NADPH bound in the regulatory site retards dissociation of $NADP^+$ from the catalytic site of EH_2NADP^+. Dissociation of $NADP^+$ induces further flavin reduction as the equilibrium adjusts in favour of the EH_2 form of FprA. The presence of NADPH in the regulatory site hinders dissociation of $NADP^+$ from the catalytic site and so retards the flavin reduction rate. Clearly the regulatory site has a lower affinity for NADPH than does the catalytic site, so permitting hydride transfer to occur more rapidly at low [NADPH]. The final product of the reaction is hydroquinone FprA with NADPH bound (EH_2NADPH) (Scheme 1A). The absence of kinetic evidence for a regulatory site in reactions with NADH means that flavin reduction can be modelled using the rapid equilibrium assumption of Strickland et al. [43] (Scheme 1C; Figure 5A).

In the oxidative reaction of EH_2 with $NADP^+$ (as studied by single-wavelength and PDA stopped-flow), it appears that the enzyme is largely freed from the regulatory effects of the second NADPH-binding site (perhaps reflecting also that $NADP^+$ has rather lower affinity than NADPH for this site) and that the oxidative process can occur at least as fast as the reductive reaction, despite the thermodynamic barrier (Figure 4). The final spectral species formed for both the reductive (oxidized FprA plus NADPH) and oxidative (hydroquinone FprA plus $NADP^+$) reactions (at the same concentrations of FprA and pyridine nucleotide) are essentially identical, indicating that the same final redox state of FprA is achieved in both cases, with substantial population of the blue semiquinone species. As also proposed by Fischer and co-workers [19], we envisage that this accumulates by the comproportionation reaction between a CT species (E_{ox}NADPH) and the final product of the reductive reaction EH_2NADPH, forming two molecules of NADPH-bound semiquinone FprA (E_{sq}NADPH) (Scheme 1B). This reaction occurs slowly, and we demonstrate (as expected) that the process is [FprA]-dependent (Figure 8). Studies on the mammalian ADR enzymes have revealed some notable similarities to FprA, and most striking is the fact that flavin semiquinone is also obtained in reductive titrations with NADPH [44]. As with FprA, formation of ADR semiquinone has been attributed to comproportionation between molecules of ADR existing as (1) a CT complex between reduced ADR and $NADP^+$ (or oxidized ADR and NADPH), and (2) reduced ADR with NADPH bound. In this way, two molecules of ADR with semiquinone flavin (both bound to NADPH) can form [45].

In future studies, we aim to examine the NADPH-binding site of FprA using a combination of molecular modelling, structural biology and mutagenesis/kinetics in order to define better the unusual NADPH-dependence observed in FprA and (apparently) replicated in NOS and CPR. The acceleration of hydride transfer to the FAD in FprA is far more marked than in NOS or CPR, and this simpler flavoenzyme might prove a more tractable model system to study the regulation of hydride transfer. The atomic structures of $NADP^+$- and NADPH-bound forms of FprA reveal the presence of two arginine residues (Arg^{199} and Arg^{200}) in close proximity to the 2′-phosphate group of the nicotinamide nucleotide cofactor ([18]; Protein Data Bank numbers 1LQT and 1LQU). In previous studies we have demonstrated roles for a cluster of arginine residues in control of NADPH binding and hydride transfer in *E. coli* flavodoxin reductase [32]. We consider that these residues may be key to $NADP^+$(H) binding and essential to the regulatory effects observed at high [NADPH], making them attractive for mutagenesis studies.

In conclusion, we have expressed the Mtb ADR homologue FprA and analysed its spectroscopic, thermodynamic and kinetic features. FprA displays similar redox properties to other related flavoprotein reductases, but exhibits intriguing discrimination between NADH and NADPH cofactors as regards the hydride transfer reaction to the FAD flavin. Although there is a positive and hyperbolic dependence of flavin reduction rate on [NADH], the situation with NADPH is quite different. Flavin reduction rate is markedly increased at lower [NADPH], which we ascribe to diminished population of a second inhibitory binding site for NADPH. This phenomenon has been observed previously in NOS and CPR, but is more clearly observed in FprA, where a >6-fold enhancement of flavin reduction is observed at low [NADPH].

We would like to thank the Biotechnology and Biological Sciences Research Council and European Union (Project 'X-TB') for financial support for these studies. We are also grateful to Professor Stewart Cole (Institut Pasteur) for provision of cosmid DNA and for helpful scientific discussions. We would also like to thank Professor Nicholas Price and Dr Sharon Kelly (University of Glasgow) for access to facilities for CD spectroscopy and for helpful discussions, and Dr Myles Cheesman (University of East Anglia) for access to EPR facilities and helpful interpretations. Thanks are also due to Dr Alessandro Aliverti and Dr Frederico Fischer (University of Milan) for provision of FprA samples used in preliminary redox potentiometry studies. N.S.S. is a Lister Institute Research Professor.

REFERENCES

1 Anti-tuberculosis drug resistance in the world (1997) The WHO/IUTALD global project on anti-tuberculosis drug resistance surveillance, WHO (http://www.who.int/gtb/publications/dritw/index.htm)

2 Zhang, Y. and Young, D. B. (1993) Molecular mechanisms of isoniazid: a drug at the front line of tuberculosis control. Trends Microbiol. **1**, 109–113
3 Baulard, A. R., Betts, J. C., Engohang-Ndong, J., Quan, S., McAdam, R. A., Brennan, P. J., Locht, C. and Besra, G. S. (2000) Activation of the pro-drug ethionamide is regulated in mycobacteria. J. Biol. Chem. **275**, 28326–28331
4 Cole, S. T., Brosch, R., Parkhill, J., Garnier, T., Churcher, C., Harris, D., Gordon, S. V., Eiglmeier, K., Gas, S., Barry, C. E. et al. (1998) Deciphering the biology of *Mycobacterium tuberculosis* from the complete genome sequence. Nature (London) **393**, 537–544
5 Daffe, M. and Draper, P. (1998) The envelope layers of mycobacteria with reference to their pathogenicity. Adv. Microbial. Physiol. **39**, 131–203
6 Podust, L. M., Poulos, T. L. and Waterman, M. R. (2001) Crystal structure of cytochrome P450 14α-sterol demethylase (CYP51) from *Mycobacterium tuberculosis* in complex with azole inhibitors. Proc. Natl. Acad. Sci. U.S.A. **98**, 3068–3073
7 Leys, D., Mowat, C. G., McLean, K. J., Richmond, A., Chapman, S. K., Walkinshaw, M. D. and Munro, A. W. (2003) Atomic structure of *Mycobacterium tuberculosis* CYP121 to 1.06 Å reveals novel features of cytochrome P450. J. Biol. Chem. **278**, 5141–5147
8 Bentley, S. D., Chater, K. F., Cerdeno-Tarraga, A. M., Challis, G. L., Thomson, N. R., James, K. D., Harris, D. E., Quail, M. A., Kieser, H., Harper, D. et al. (2002) Complete genome sequence of the model actinomycete *Streptomyces coelicolor* A3(2). Nature (London) **417**, 141–147
9 McLean, K. J., Marshall, K. R., Richmond, A., Hunter, I. S., Fowler, K., Kieser, T., Gurcha, S. S., Besra, G. S. and Munro, A. W. (2002) Azole antifungals are potent inhibitors of cytochromes P450 and bacterial growth in mycobacteria and streptomycetes. Microbiology **148**, 2937–2949
10 McLean, K. J., Cheesman, M. R., Rivers, S. L., Richmond, A., Leys, D., Chapman, S. K., Reid, G. A., Price, N. C., Kelly, S. M., Clarkson, J. et al. (2002) Expression, purification and spectroscopic characterization of the cytochrome P450 CYP121 from *Mycobacterium tuberculosis*. J. Inorg. Biochem. **91**, 527–541
11 Guengerich, F. P., Hosea, N. A., Parikh, A., Bell-Parikh, L. C., Johnson, W. W., Gillam, E. M. J. and Shimada, T. (1998) Twenty years of biochemistry of human P450s: purification, expression, mechanism, and relevance to drugs. Drug Met. Dispos. **26**, 1175–1178
12 Gutierrez, A., Lian, L. Y., Wolf, C. R., Scrutton, N. S. and Roberts, G. C. K. (2001) Stopped-flow kinetic studies of flavin reduction in human cytochrome P450 reductase and its component domains. Biochemistry **40**, 1964–1975
13 Munro, A. W. and Lindsay, J. G. (1996) Bacterial cytochromes P450. Mol. Microbiol. **20**, 1115–1125
14 Pikuleva, I. A., Mackman, R. L., Kagawa, N., Waterman, M. R. and Ortiz de Montellano, P. R. (1995) Active site topology of bovine cholesterol side chain cleavage cytochrome P450 (P450scc) and evidence for interaction of tyrosine 94 with the side chain of cholesterol. Arch. Biochem. Biophys. **322**, 189–197
15 Ziegler, G. A. and Schulz, G. E. (2000) Crystal structures of adrenodoxin reductase in complex with $NADP^+$ and NADPH suggesting a mechanism for the electron transfer of an enzyme family. Biochemistry **39**, 10986–10995
16 Grinberg, A. V., Hannemann, F., Schiffler, B., Muller, J., Heinemann, U. and Bernhardt, R. (2000) Adrenodoxin: Structure, stability, and electron transfer properties. Proteins: Struct., Funct., Genet. **40**, 590–612
17 Muller, J. J., Lapko, A., Bourenkov, G., Ruckpaul, K. and Heinemann, U. (2001) Adrenodoxin reductase–adrenodoxin complex structure suggests electron transfer path in steroid biosynthesis. J. Biol. Chem. **276**, 2786–2789
18 Bossi, R. T., Aliverti, A., Raimondi, D., Fischer, F., Zanetti, G., Ferrari, D., Tahallah, N., Maier, C. S., Heck, A. J. R., Rizzi, M. and Mattevi, A. (2002) A covalent modification of $NADP^+$ revealed by the atomic resolution structure of FprA, a *Mycobacterium tuberculosis* oxidoreductase. Biochemistry **41**, 8807–8818
19 Fischer, F., Raimondi, D., Aliverti, A. and Zanetti, G. (2002) *Mycobacterium tuberculosis* FprA, a novel bacterial NADPH-ferredoxin reductase. Eur. J. Biochem. **269**, 3005–3013
20 Gibson, T. J. (1984) Studies in the Epstein-Barr virus genome. PhD Thesis, University of Cambridge, U.K.
21 Sambrook, J., Fritsch, E. F. and Maniatis, T. (1989) Molecular Cloning: A Laboratory Manual, 2nd ed., Cold Spring Harbor Laboratory Press, Cold Spring Harbor, NY
22 Munro, A. W. and Noble, M. A. (1999) Fluorescence analysis of flavoproteins. In Flavoprotein Protocols, (Chapman, S. K. and Reid, G. A., eds), pp. 25–48, Humana Press, Totowa, NJ
23 Munro, A. W., Noble, M. A., Robledo, L., Daff, S. N. and Chapman, S. K. (2001) Determination of the redox properties of human NADPH-cytochrome P450 reductase. Biochemistry **40**, 1956–1963
24 Dutton, P. L. (1978) Redox potentiometry: determination of midpoint potentials of oxidation-reduction components of biological electron-transfer systems. Methods Enzymol. **54**, 411–435
25 Ost, T. W. B., Miles, C. S., Munro, A. W., Murdoch, J., Reid, G. A. and Chapman, S. K. (2001) Phenylalanine 393 exerts thermodynamic control over the heme of flavocytochrome P450BM3. Biochemistry **40**, 13421–13429
26 Tew, D. G. (1993) Inhibition of cytochrome P450 reductase by the diphenyliodonium cation. Kinetic analysis and covalent modifications. Biochemistry **32**, 10209–10215
27 McIver, L., Leadbeater, C., Campopiano, D. J., Baxter, R. L., Daff, S. N., Chapman, S. K. and Munro, A. W. (1998) Characterisation of flavodoxin $NADP^+$ oxidoreductase and flavodoxin; key components of electron transfer in *Escherichia coli*. Eur. J. Biochem. **257**, 577–585
28 Studier, F. W. and Moffatt, B. A. (1986) Use of bacteriophage T7 RNA-polymerase to direct selective high-level expression of cloned genes. J. Mol. Biol. **189**, 113–130
29 Reference deleted
30 Suhara, K., Ikeda, Y., Takemori, S. and Katagiri, M. (1972) The purification and properties of NADPH-adrenodoxin reductase from bovine adrenocortical mitochondria. FEBS Lett. **28**, 45–48
31 Pederson, J. I. and Godager, H. K. (1978) Purification of NADPH-ferredoxin reductase from rat liver mitochondria. Biochim. Biophys. Acta **525**, 28–33
32 Leadbeater, C., McIver, L., Campopiano, D. J., Webster, S. P., Baxter, R. L., Kelly, S. M., Price, N. C., Lysek, D. A., Noble, M. A., Chapman, S. K. and Munro, A. W. (2000) Probing the NADPH-binding site of *Escherichia coli* flavodoxin oxidoreductase. Biochem. J. **352**, 257–266
33 Daff, S. N., Chapman, S. K., Turner, K. L., Holt, R. A., Govindaraj, S., Poulos, T. L. and Munro, A. W. (1997) Redox control of the catalytic cycle of flavocytochrome P-450 BM3. Biochemistry **36**, 13816–13823
34 McLean, K. J., Scrutton, N. S., Munro, A. W., Fischer, F. and Aliverti, A. (2002) Expression and thermodynamic characterization of the *Mycobacterium tuberculosis* adrenodoxin reductase homologue: FprA. In Flavins and Flavoproteins 2002: Proceedings of the 14th International Symposium on Flavins and Flavoproteins (Scrutton, N. S., Chapman, S. K. and Perham, R., eds), pp. 605–610, Rudolf Weber, Berlin
35 Murataliev, M. B. and Feyereisen, R. (2000) Interaction of NADP(H) with oxidized and reduced P450 reductase during catalysis, studies with nucleotide analogues. Biochemistry **39**, 5066–5074
36 Aliverti, A., Fischer, F., Pasquini, S., Vanoni, M. A., Curti, B., Zanetti, G., Cantoni, R., Branzoni, M. and Riccardi, G. (1999) Characterization of an adrenodoxin reductase-like protein of Mycobacterium tuberculosis. In Flavins and Flavoproteins 1999: Proceedings of the 13th International Symposium on Flavins and Flavoproteins. (Ghisla, S., Kroneck, P., Macheroux, P. and Sund, H., eds), pp. 891–894, Rudolf Weber, Berlin
37 Gutierrez, A., Paine, M., Wolf, C. R., Scrutton, N. S. and Roberts, G. C. K. (2002) Relaxation kinetics of cytochrome P450 reductase: internal electron transfer is limited by conformational change and regulated by coenzyme binding. Biochemistry **41**, 4626–4637
38 Knight, K. and Scrutton, N. S. (2002) Stopped-flow kinetic studies of electron transfer in the reductase domain of neuronal nitric oxide synthase: re-evaluation of the kinetic mechanism reveals new enzyme intermediates and variation with cytochrome P450 reductase. Biochem. J. **367**, 19–30
39 Nelson, D. R., Koymans, L., Kamataki, T., Stegeman, J. J., Feyereisen, R., Waxman, D. J., Waterman, M. R., Gotoh, O., Coon, M. J., Estabrook, R. W. et al. (1996) P450 superfamily: update on new sequences, gene mapping, accession numbers and nomenclature. Pharmocogenetics **6**, 1–42
40 Takeuchi, K., Tsubaki, M., Futagawa, J., Masuya, F. and Hori, H. (2001) Adrenodoxin-cytochrome P450scc interaction as revealed by EPR spectroscopy: comparison with the putidaredoxin-cytochrome P450cam system. J. Biochem. (Tokyo) **130**, 789–797
41 Bellamine, A., Mangla, A. T., Nes, W. D. and Waterman, M. R. (1999) Characterization and catalytic properties of the sterol 14α-demethylase from *Mycobacterium tuberculosis*. Proc. Natl. Acad. Sci U.S.A. **96**, 8937–8942
42 Craig, D. H., Chapman, S. K. and Daff, S. (2002) Calmodulin activates electron transfer through neuronal nitric-oxide synthase reductase domain by releasing an NADPH-dependent conformational lock. J. Biol. Chem. **277**, 33987–33994
43 Strickland, S., Palmer, G. and Massey, V. (1975) Determination of dissociation constants and specific rate constants of enzyme-substrate (or protein-ligand) interactions from rapid reaction data. J. Biol. Chem. **250**, 4048–4052
44 Lambeth, J. D. and Kamin, H. (1976) Adrenodoxin reductase: properties of complexes of reduced enzyme with $NADP^+$ and NADPH. J. Biol. Chem. **251**, 4299–4306
45 Nonaka, Y., Fujii, S. and Yamano, T. (1986) The semiquinone state of NADPH-adrenodoxin reductase in the course of anaerobic reduction with NADPH. J. Biochem. (Tokyo) **99**, 803–814

Received 30 October 2002/28 February 2003; accepted 3 March 2003
Published as BJ Immediate Publication 3 March 2003, DOI 10.1042/BJ20021692